SIAM REVIEW
Vol. 41, No. 1, pp. 115–131

Periodic Folding of Thin Sheets*

L. Mahadevan†
Joseph B. Keller‡

Abstract. When a thin sheet of a flexible material such as paper is fed from a horizontal spool towards a rough horizontal plane below it, the sheet folds on itself in a regular manner. We model this phenomenon as a free boundary problem for a nonlinearly elastic sheet, taking into account the stiffness and weight of the sheet and the height of the spool above the plane. By using a continuation scheme we solve the problem numerically and follow the evolution of one period of the fold for various values of the parameters. The results are found to agree well with observations of the folding of paper sheets.

Key words. nonlinear elasticity, contact, free boundary problems

AMS subject classifications. 34B15, 34E10, 65L10, 73C50, 73H05

PII. S0036144598339166

1. Introduction.

When a thin sheet of a flexible material such as paper is fed uniformly from a horizontal spool towards a horizontal solid plane below it, the sheet folds on itself in a regular manner. Variants of this phenomenon occur in the manufacturing of papers, textiles, and composite sheets [1], and in the creeping flow of viscous liquids [2], [3].

Observations of a sheet that is fed slowly from far above a horizontal floor reveal various stages in the formation of one half-period of a fold. Figures 1a–1i show these stages for a sheet of paper as it is unrolled from a spool held above the floor and photographed along a horizontal axis parallel to the generators of the sheet.

Suppose that the sheet is fed from the spool starting at a time $t = 0$. Then it hangs vertically under the influence of gravity until it touches the floor $y = 0$ along a line of contact $x = 0$ at a time $t = t_0$. Further feeding causes the sheet to buckle. Most of the deformation is limited to a narrow layer near the floor (Figure 1a). If the plane is rough, the sheet does not slip and the contact line remains at $x = 0$. The sheet buckles some more as the feeding continues, eventually becoming tangential to the horizontal plane at a time $t = t_1$ (Figure 1b). The line where the sheet leaves the floor, i.e., the contact line, then begins to move away from its initial position $x = 0$ (Figure 1c) as more of the sheet is fed. This continues until the contact line reaches a maximum distance from $x = 0$ (Figure 1d) and then begins to move back toward it (Figure 1e). Simultaneously, the line of inflection in the sheet begins to move towards the floor, and the sheet finally touches itself at a time $t = t_2$ (Figure 1f). If the sheet is rough it cannot slide through the line of contact. Instead, further feeding

*Published electronically January 22, 1999. This paper originally appeared in *SIAM Journal on Applied Mathematics*, Volume 55, Number 6, 1995, pages 1609 to 1624.
http://www.siam.org/journals/sirev/41-1/33916.html

†Division of Mechanics and Materials, Department of Mechanical Engineering, 1-310, Massachusetts Institute of Technology, Cambridge, MA 02139 (l_m@mit.edu).

‡Departments of Mathematics and Mechanical Engineering, Stanford University, Stanford, CA 94305 (keller@math.stanford.edu).

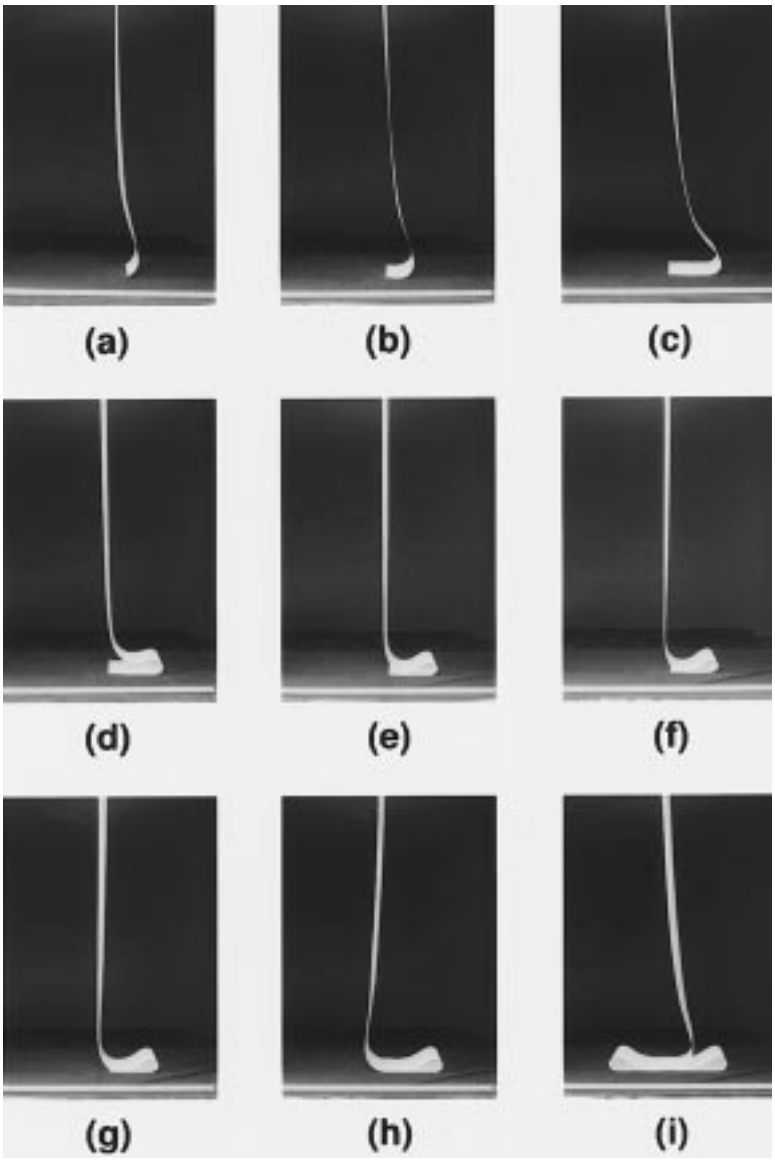

Fig. 1 *Photographs of the evolution of an entire fold of a sheet of paper fed vertically from far above a rough horizontal floor. The ruler at the bottom of each photograph is* 1 m *long. The various stages illustrated show the sheet* (a) *just after it touches the floor and buckles,* (b) *when it just becomes tangential to the floor,* (c) *when it has been laid out after the line of tangency has moved away from its original position,* (d) *when it is in its extreme configuration,* (e) *when it starts to roll back,* (f) *when it first touches itself on the floor and forms a second contact line,* (g) *when it is rolling about the second contact line,* (h) *at the end of one half-period, and* (i) *at the end of a full period.*

causes the sheet to roll about the second contact line as this line moves toward the feeding plane. This rolling continues until the curvature along the second contact line becomes zero at a time $t = t_3$ (Figure 1g). Then the second contact line stops moving and a folded portion of the sheet held down by its own weight is left behind. As more

of the sheet is laid out, a third contact line splits off from where the second contact line stopped, starts to move, and arrives at $x = 0$ at a time $t = t_4$ (Figure 1h). Then the hanging part of the sheet is in the same configuration as at time $t = t_1$ (Figure 1b) except for a reflection about the vertical plane $x = 0$. As the feeding continues, another half-period of the fold is laid out in exactly the same manner (Figure 1i). Thus it suffices to consider the evolution of a half-period of a fold. Of course, during the evolution of the second fold, the sheet lies on top of the first fold. For very flexible sheets the fold height is small, so this effect is small. Therefore we shall not consider it.

In section 2 we use dimensional analysis to extract the appropriate dimensionless parameters in the problem. We then formulate a free boundary value problem for the quasi-static evolution of one half-period of a fold. In section 3 we describe a numerical method to solve the boundary value problem and follow the formation of a fold. We present the results for various parameter values. In section 4 we obtain a solution for a free-standing fold held down by its own weight. Finally, in section 5 we present some quantitative comparisons of our calculated results with the results of experiments using paper sheets.

2. Formulation.

2.1. Dimensional Analysis. To understand the role of the various physical parameters in the problem, we use dimensional analysis. The six parameters are the Young's modulus E, the mass per unit length ρ of unit width of the sheet, the moment of inertia I of the cross section of unit width of the sheet, the height l of the spool above the solid plane, the feeding velocity v, and the acceleration of gravity g. Their dimensions are expressible in terms of mass, length, and time. Therefore, by the Buckingham Pi theorem, the number of dimensionless parameters is three, say,

$$\begin{aligned} \eta &= EI/\rho g l^3, \\ \gamma &= v^2/gl, \\ \zeta &= I/l^3. \end{aligned} \tag{2.1}$$

Here η is the dimensionless stiffness given by the ratio of the flexural and gravitational potential energies, γ is the ratio of the kinetic and potential energies, and ζ is the dimensionless moment of inertia. Thus the fold length l_f measured along the arc, divided by l, is a function of these three parameters, $l_f/l = g(\eta, \gamma, \zeta)$.

When the sheet is fed slowly so that inertial forces are negligible, $\gamma << 1$. For typical materials, $\eta >> \zeta$ and $\zeta << 1$ so that

$$l_f = lg(\eta, \gamma, \zeta) \sim lg(\eta, 0, 0). \tag{2.2}$$

As the drop height l is increased indefinitely, for l_f to have a finite limit, $g(\eta, 0, 0)$ must be proportional to $\eta^{1/3}$, and then (2.2) becomes

$$l_f \sim Ll\eta^{1/3} = L(EI/\rho g)^{1/3}. \tag{2.3}$$

The constant L can be found from one calculation or from one experiment.

For a thin sheet of paper, typical parameter values are

$$\begin{aligned} E &\sim 3 \times 10^8 N/m^2, & I &\sim 1/3 \times 10^{-12} m^4, \\ \rho &\sim 10^{-1} kg/m, & g &\sim 10 m/s^2, \quad l \sim 1m. \end{aligned} \tag{2.4}$$

Then $\eta = 10^{-3}$. Therefore, the effect of the stiffness will be important only in the boundary layers near the feeding point and near the horizontal plane.

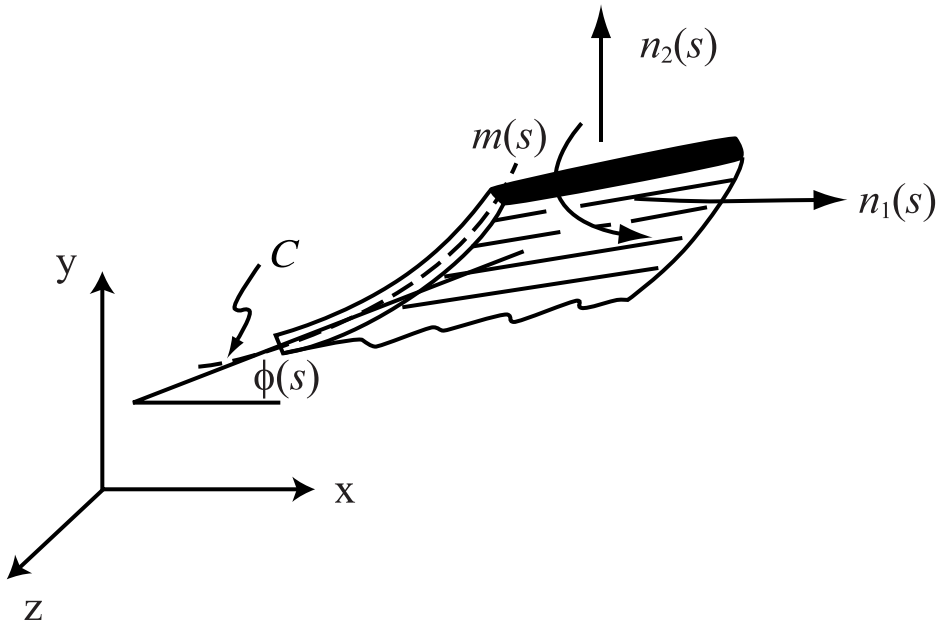

Fig. 2. *The geometry and loading of a cylindrical sheet whose generators are parallel to the z axis.*

2.2. Equations of Equilibrium. We assume that the sheet is cylindrical with its generators parallel to the z axis, so that it is determined by its curve of intersection C with the xy plane. When γ is sufficiently small, inertial forces are negligible and the equations of motion become those of equilibrium.

They are the same as those for the bending of a naturally straight rod lying in the xy plane (see Figure 2). The balance of forces in this plane and the balance of moments normal to it give the equations [4]

$$\begin{aligned} n_{1s} &= 0, \qquad 0 \le s \le vt, \\ n_{2s} &= \rho g, \\ m_s &= n_1 \sin\phi - n_2 \cos\phi. \end{aligned} \tag{2.5}$$

Here s is the arc-length along C, $\phi(s)$ is the angle between the tangent to C and the x axis, $n_1(s)$ and $n_2(s)$ are the stress resultants in the x and y directions, $m(s)$ is the bending moment in the z direction, ρg is the weight per unit length of unit width of the sheet, and vt is the length of the sheet. As in Bernoulli–Euler beam theory, we assume that $m(s) = EI\phi_s(s)$, where EI is the flexural stiffness of the sheet. The x and y coordinates of C are determined by

$$\begin{aligned} x_s &= \cos\phi, \qquad 0 \le s \le vt, \\ y_s &= \sin\phi. \end{aligned} \tag{2.6}$$

This simple model of geometrically nonlinear elasticity is a good approximation for the behavior of thin sheets undergoing only planar bending in the absence of extension, shear, and warping. If gravity were not present, $n_2(s)$ would be a constant and the problem would reduce to that of the classical elastica of Euler. However here gravity is important and cannot be neglected.

We now define the dimensionless variables

$$\begin{aligned} \bar{s} &= s/l, & \bar{t} &= vt/l, \\ \bar{x} &= x/l, & \bar{y} &= y/l, \\ \bar{n_1} &= n_1/\rho g l, & \bar{n_2} &= n_2/\rho g l. \end{aligned} \tag{2.7}$$

Then we can rewrite (2.5) and (2.6), after dropping the bars, as follows:

$$\begin{aligned} n_{1s} &= 0, & 0 \le s \le t, \\ n_{2s} &= 1, \\ \eta\phi_{ss} &= n_1 \sin\phi - n_2 \cos\phi, \\ x_s &= \cos\phi, \\ y_s &= \sin\phi. \end{aligned} \tag{2.8}$$

This forms a sixth-order system of ordinary differential equations for the variables n_1, n_2, x, y, and ϕ as functions of s.

2.3. Boundary Conditions. Suppose the spool is at a height l above the horizontal plane and that the sheet leaves it vertically. Therefore, at the spool $s = vt$, or $\bar{s} = \bar{t}$, we have

$$\begin{aligned} x(t) &= 0, & t \ge 0, \\ y(t) &= l, \\ \phi(t) &= \pi/2. \end{aligned} \tag{2.9}$$

Recalling the observations in section 1, we note that there are four switching points where the boundary conditions at the other end of the sheet change. These switching points correspond to the birth and motion of the contact lines shown in Figure 1. For $0 \le t \le 1$, the sheet hangs vertically with its bottom end free. At the end $s = 0$, we have

$$\begin{aligned} n_1(0;t) &= 0, & 0 \le t \le 1, \\ n_2(0;t) &= 0, \\ y(0;t) &= 1 - t. \end{aligned} \tag{2.10}$$

At $t = 1$, the sheet touches the horizontal plane and further feeding causes it to buckle (Figure 1a). In the presence of friction, the line of contact remains fixed, acting as a hinged support about which the sheet bends. Then the conditions (2.10) are replaced by

$$\begin{aligned} x(0;t) &= 0, & 1 \le t \le t_1, \\ y(0;t) &= 0, \\ \phi_s(0;t) &= 0. \end{aligned} \tag{2.11}$$

At $t = t_1$ the sheet becomes tangent to the plane at $s = 0$. Then $\phi(0;t_1) = 0$ (Figure 1b). As the feeding continues, the sheet gets laid out along the horizontal plane (Figure 1c). At the first contact line $(s_1(t), 0)$, where the sheet leaves the floor,

$$\begin{aligned} y(s_1;t) &= 0, & t_1 \le t \le t_2, \\ \phi(s_1;t) &= 0, \\ \phi_s(s_1;t) &= 0. \end{aligned} \tag{2.12}$$

As the contact line moves, the sheet begins to dip downwards under its own weight. At $t = t_2$ a second contact line forms at $(x(s_2(t);t), 0)$ when the sheet touches itself (Figure 1f). Further feeding causes the sheet to roll back about the second contact line which moves towards $x = 0$. The first contact line may also move during this process. However, in the presence of friction this motion is very small. For simplicity we neglect it. During this rolling motion, a line reaction is exerted by the horizontal plane along the second contact line, causing a jump in the vertical force $n_2(s)$ at $s = s_2(t)$. At the second contact line,

$$\begin{aligned} y(s_2;t) &= 0, \qquad t_2 \le t \le t_3, \\ \phi(s_2;t) &= \pi. \end{aligned} \tag{2.13}$$

The sheet continues to roll about $(x(s_2(t);t), 0)$ until the curvature $\phi_s(s_2(t);t)$ at the second contact line becomes zero (Figure 1g). This happens at $t = t_3$. Then a folded portion of the sheet from $s_1(t_2)$ to $s_2(t_3)$ is left behind and a new contact line $(x_3(t), 0)$, initially at $(x(s_2(t_3)), 0)$, moves toward $x = 0$. At this contact line

$$\begin{aligned} y(s_3;t) &= 0, \qquad t_3 \le t \le t_4, \\ \phi_s(s_3;t) &= 0, \\ \phi(s_3;t) &= \pi. \end{aligned} \tag{2.14}$$

Further feeding causes the third contact line to move towards $x = 0$ until it reaches $x = 0$ at $t = t_4$. Then the configuration of the hanging portion is identical to that at $t = t_1$ except for a reflection about the y axis. A similar process then leads to the laying out of the second half-period of the fold, and an entire period is completed at $t = 1 + 2(t_4 - t_1)$. Thus it suffices to determine one half-period of a fold by solving (2.8) subject to the boundary conditions (2.9)–(2.14).

3. The Evolution of a Fold.

3.1. Solution by Perturbation. The vertical sheet just touches the horizontal plane at $t = 1$. Further feeding causes it to buckle out of the vertical plane. We can calculate the buckled solution at $t = 1 + \epsilon$, $\epsilon << 1$ by expansion in ϵ. For simplicity we omit gravity and write

$$\begin{aligned} \phi(s;\epsilon) &= \pi/2 - \epsilon\hat{\phi} + O(\epsilon^2), \\ n_1(s;\epsilon) &= \epsilon\hat{n_1} + O(\epsilon^2), \\ n_1(s;\epsilon) &= n_2^0 + \epsilon\hat{n_2} + O(\epsilon^2), \\ x(s;\epsilon) &= \epsilon\hat{x} + O(\epsilon^2), \\ y(s;\epsilon) &= s + \epsilon\hat{y} + O(\epsilon^2). \end{aligned} \tag{3.1}$$

Upon substituting (3.1) into (2.8) and (2.10) and keeping terms to $O(\epsilon)$, we get

$$\begin{aligned} \hat{n}_{1s} &= 0, \\ \hat{n}_{2s} &= 0, \\ \hat{x}_s &= -\hat{\phi}, \\ \hat{y}_s &= 0, \\ -\eta\hat{\phi}_{ss} &= \hat{n}_1 - n_2^0\hat{\phi}, \end{aligned} \tag{3.2}$$

subject to the boundary conditions

$$\begin{aligned} \hat{x}(0) &= 0, \\ \hat{y}(0) &= 0, \\ \hat{\phi}_s(0) &= 0, \\ \hat{x}(0) &= 0, \\ \hat{y}(1) &= 0, \\ \hat{\phi}_s(1) &= 0. \end{aligned} \tag{3.3}$$

Solving (3.2)–(3.3) and substituting into (3.1) yields the buckled solution

$$\begin{aligned} n_1(s;\epsilon) &= O(\epsilon^2), \\ n_2(s;\epsilon) &= j^2\eta\pi^2 + O(\epsilon^2), \quad j = 1, 2, \ldots, \\ \phi(s;\epsilon) &= \pi/2 - \epsilon\cos j\pi s + O(\epsilon^2), \\ x(s;\epsilon) &= \frac{\epsilon}{j\pi}\sin j\pi s + O(\epsilon^2), \\ y(s;\epsilon) &= s + O(\epsilon^2). \end{aligned} \tag{3.4}$$

We shall use (3.4) with $j = 1$ as an initial approximation in a numerical iterative procedure to solve the boundary value problem with gravity for $t = 1+\epsilon$. Then we shall use that solution as an initial approximation to solve the problem for $t = 1 + 2\epsilon$, and so on. This procedure constitutes a continuation or homotopy method parametrized by the sheet length t.

3.2. Numerical Scheme. At each step of the continuation scheme we use a numerical boundary value problem solver COLSYS [5] to compute the solution. It uses spline collocation at Gaussian points. A brief description of the method is as follows: by forcing a collocation solution to satisfy the boundary conditions and the differential equations at the Gauss–Legendre points in a defined mesh, a nonlinear system of equations is obtained for the unknown B-spline coefficients. A damped quasi-Newton method is used to solve the nonlinear system iteratively starting from an initial approximation to the solution. A posteriori error estimates are used to refine the mesh adaptively until the specified tolerances are met. The spline coefficients of the collocation solution are stored to allow for the possibility of simple continuation. In the absence of singular points such as bifurcation or fold points, the continuation algorithm simply involves solving a sequence of nonlinear problems. Then each solution gives an initial approximation to the solution at the next step.

To facilitate the use of COLSYS, we convert the original problem with moving boundaries to one with fixed boundaries. This is done by writing the equations in terms of a new variable $\hat{s} = (s - s_1)/(t - s_1)$, where s_1 is the x coordinate of the contact line and t is the dimensionless length of the sheet. Then, on dropping the hats, we can rewrite (2.8) as

$$\begin{aligned} n_{1s} &= 0, \qquad 0 \le s \le 1, \\ n_{2s} &= t - s_1, \\ \eta\phi_{ss} &= (t - s_1)^2(n_1\sin\phi - n_2\cos\phi), \\ x_s &= (t - s_1)\cos\phi, \\ y_s &= (t - s_1)\sin\phi, \\ s_{1s} &= 0. \end{aligned} \tag{3.5}$$

The last equation serves to embed the sixth-order system with a free boundary in a seventh-order system with fixed boundaries, which requires the specification of an additional boundary condition to complete the formulation of the problem.

The boundary conditions (2.9)–(2.14) at $s = 0$, $s = s_1$, and $s = t$ are transformed into conditions at $\hat{s} = 0$ and $\hat{s} = 1$. At the feeding end, $s = t$ or $\hat{s} = 1$, (2.9) can be rewritten as

$$\begin{aligned} x(1;t) &= 0, \qquad t \geq 0, \\ y(1;t) &= 1, \\ \phi(1;t) &= \pi/2. \end{aligned} \tag{3.6}$$

At the other end, $s = 0$ or $\hat{s} = 0$, (2.10) is transformed into

$$\begin{aligned} n_1(0;t) &= 0, \qquad 0 \leq t \leq 1, \\ n_2(0;t) &= 0, \\ y(0;t) &= 1 - t, \\ s_1(t) &= 0, \end{aligned} \tag{3.7}$$

while (2.11) becomes

$$\begin{aligned} x(0;t) &= 0, \qquad 1 \leq t \leq t_1, \\ y(0;t) &= 0, \\ \phi_s(0;t) &= 0, \\ s_1(t) &= 0. \end{aligned} \tag{3.8}$$

Once the sheet begins to get laid out on the plane, $s_1(t) \neq 0$. At the contact line, $s = s_1$ or $\hat{s} = 0$, (2.12) becomes

$$\begin{aligned} x(0;t) &= s_1, \qquad t_1 \leq t \leq t_2, \\ y(0;t) &= 0, \\ \phi_s(0;t) &= 0, \\ \phi(0;t) &= 0. \end{aligned} \tag{3.9}$$

The second contact line is formed when $t = t_2$. Thereafter, the boundary conditions (2.13) at $s = s_2(t)$ or $\hat{s} = (s_2 - s_1)/(t - s_1)$ are transformed to

$$\begin{aligned} y\left(\frac{s_2 - s_1}{t - s_1}; t\right) &= 0, \qquad t_2 \leq t \leq t_3, \\ \phi\left(\frac{s_2 - s_1}{t - s_1}; t\right) &= \pi. \end{aligned} \tag{3.10}$$

The third contact line is formed when $t = t_3$. Thereafter, the boundary conditions (2.14) at $s = s_3(t)$ or $\hat{s} = (s_3 - s_1)/(t - s_1)$ become

$$\begin{aligned} x\left(\frac{s_3 - s_1}{t - s_1}; t\right) &= x_3, \qquad t_3 \leq t \leq t_4, \\ y\left(\frac{s_3 - s_1}{t - s_1}; t\right) &= 0, \end{aligned}$$

$$\phi\left(\frac{s_3 - s_1}{t - s_1}; t\right) = \pi,$$

$$\phi_s\left(\frac{s_3 - s_1}{t - s_1}; t\right) = 0. \tag{3.11}$$

Here $(x_3(t), 0)$ is the dimensionless position of the third contact line. It forms at the location where the second contact line stops and moves towards $x = 0$ as the sheet is fed.

To solve (3.5)–(3.11), we start with the perturbation solution given by (3.4) for $\epsilon << 1$ as an initial guess to determine the equilibrium configuration of the slightly buckled sheet in the presence of gravity. We use this solution as the first approximation in a continuation scheme parametrized by the sheet length t. As t is gradually increased past the switching point $t = t_1$, the appropriate boundary conditions given by (3.9) are enforced. At $t = t_2$, the second contact line forms, so that the interface conditions (3.10) and the boundary conditions (3.6) and (3.9) have to be satisfied. The subsequent rolling motion is more conveniently treated as a combination of two boundary value problems with matching boundary conditions given by (3.10). Once the curvature ϕ_s along the second contact line becomes zero, the third contact line begins to move and the boundary conditions (3.10) are replaced by (3.11). One half-period of the fold is competely laid out at $t = t_4$.

For a typical value of $\eta = 10^{-3}$, we choose the continuation step size for t to be $\epsilon = .01$. The adaptive remeshing scheme implemented in COLSYS automatically refines the mesh in a narrow boundary layer near the horizontal plane where most of the folding occurs. On a mesh with 40 subintervals, the quasi-Newton method takes between 3 and 5 iterations per continuation step when the error tolerances on the coordinates x and y are 10^{-5}.

3.3. Results. Figures 3a–3i show the curve of intersection C of the sheet with the xy plane at various stages during the feeding of a sheet with $\eta = 10^{-3}$ as it is fed quasi-statically. Comparison with the experimental observations of Figures 1a–1i shows good agreement. Figure 4 shows an enlarged view of the boundary layer near the horizontal plane showing the sequence of equilibria during the formation of one half-period of a fold.

Table 1 shows the location of the switching points for $t = t_1, t_2, t_3, t_4$ for three different values of the dimensionless stiffness $\eta = 10^{-3}, 10^{-4}$, and 10^{-5}. In Figures 5a–5b, the locations of the contact lines $s_i(t)$, $i = 1, 2, 3$, are shown over one period of a fold for two typical values of the dimensionless stiffness $\eta_1 = 10^{-3}$ and $\eta_2 = 10^{-4}$. We observe that the ordinates in Figures 5a and 5b are nearly identical except for a scaling factor of 2. This is in accordance with the dimensional arguments that predict that the length scales should vary asymptotically as the cube root of the dimensionless stiffness, and $(\eta_1/\eta_2)^{1/3} = 10^{1/3} \sim 2$. We also observe that for $\eta = 10^{-3}$ the sheet rolls back a smaller fraction of the fold length than for $\eta = 10^{-4}$. In fact, for large enough η, the sheet touches itself before reaching its extreme position and therefore does not roll back at all. For very small η, the fold length $l_f \sim O(\eta^{1/3})$ and all three contact lines approach each other, eventually coalescing when $\eta = 0$.

4. The Free-Standing Fold. At the end of every half-period, a free-standing fold held down by its own weight is left on the horizontal plane, as is shown in Figure 1h. We now examine the solution for this fold. The only length scale for it is the fold length l_f measured along the arc. It is given by (2.3), in which L is a constant to be

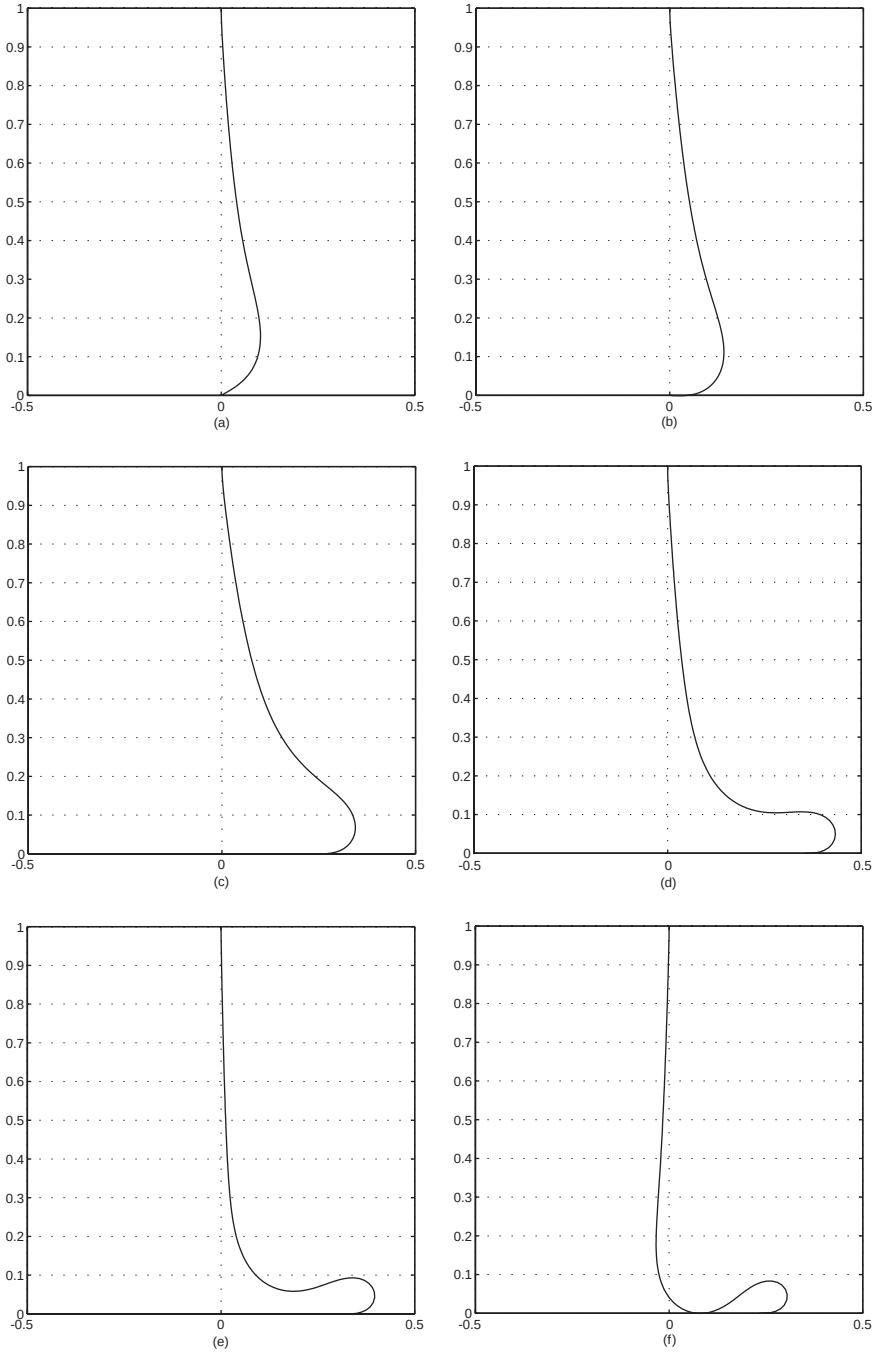

Fig. 3 *Numerical results for the evolution of an entire fold for* $\eta = 10^{-3}$ *showing the same stages as in Figure* 1. *The curve of intersection* C *of the sheet with the* xy *plane is shown for* (a) $1 \leq t \leq t_1$; (b) $t = t_1$; (c) $t_1 \leq t \leq t_2$, *as the contact line moves away from* $x = 0$; (d) $t_1 \leq t \leq t_2$, *when the contact line is at its extreme position;* (e) $t_1 \leq t \leq t_2$, *as the contact line moves towards* $x = 0$; (f) $t = t_2$; (g) $t_2 \leq t \leq t_3$; (h) $t = t_4$; *and* (i) $t = 1 + 2(t_4 - t_1)$.

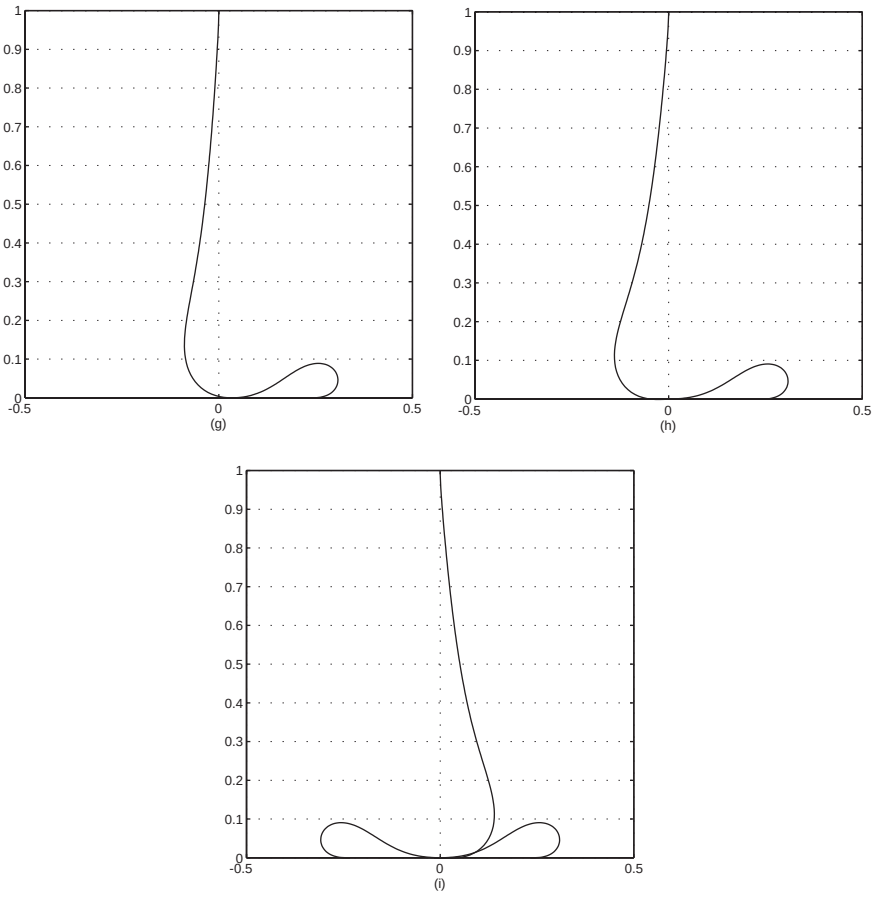

Fig. 3. *(continued)*

determined. Using l_f/L as the scaling length, we can rewrite the equations (2.5) and (2.6) in dimensionless form as

$$\begin{aligned} n_{1s} &= 0, \qquad 0 \le s \le L, \\ n_{2s} &= 1, \\ \phi_{ss} &= n_1 \sin\phi - n_2 \cos\phi, \\ x_s &= \cos\phi, \\ y_s &= \sin\phi. \end{aligned} \tag{4.1}$$

Each end of the fold lies on the horizontal plane and is tangential to it. Its curvature also vanishes at both ends. Fixing one of the ends $s = 0$ at the origin, we can write the boundary conditions as

$$\begin{aligned} x(0) &= 0, \qquad y(0) = 0, \\ \phi(0) &= \pi, \qquad \phi_s(0) = 0, \\ y(L) &= 0, \qquad \phi(L) = 0, \\ \phi_s(L) &= 0. \end{aligned} \tag{4.2}$$

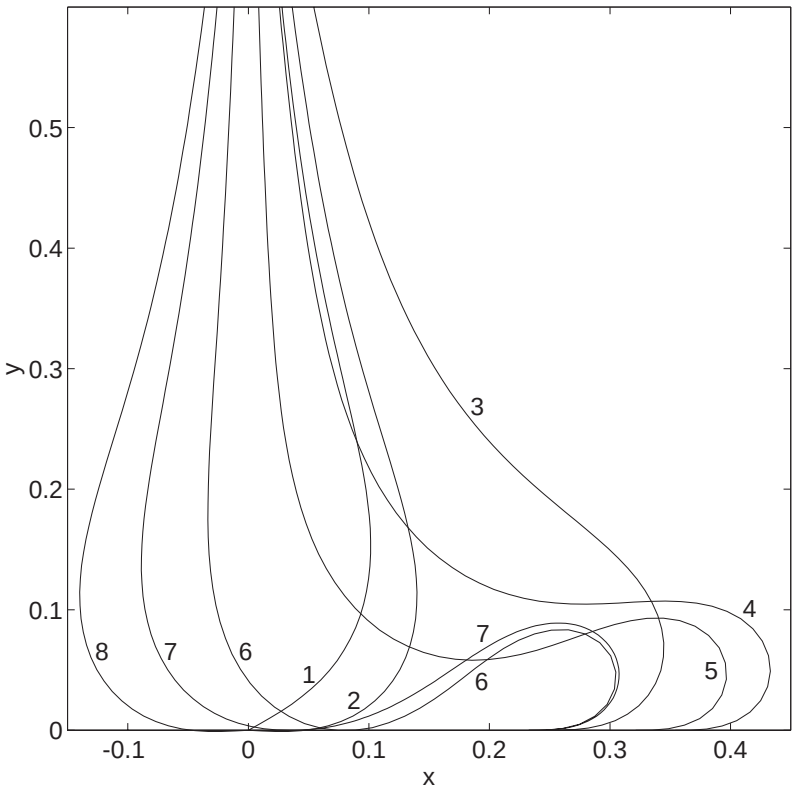

Fig. 4 *An enlarged view of the sequence of equilibria* 1–8 *during the laying out of one half-period of a fold.*

Table 1 *Location of the switching points* $t_i, i = 1, 2, 3, 4$, *and the length of one half-period* $t_4 - t_1$ *for different values of the dimensionless stiffness* η.

	$\eta = 10^{-3}$	$\eta = 10^{-4}$	$\eta = 10^{-5}$
t_1	1.105	1.053	1.023
t_2	1.912	1.313	1.154
t_3	1.973	1.499	1.268
t_4	1.993	1.508	1.271
$t_4 - t_1$	0.888	0.455	.248

Integrating the first two equations in (4.1) and substituting into the third, we get

$$\phi_{ss} + (n_2^0 + s)\cos\phi - n_1^0 \sin\phi = 0. \tag{4.3}$$

Here n_1^0 and n_2^0 are constants. Multiplying (4.3) by ϕ_s and integrating along s, we obtain

$$\frac{\phi_s^2(s)}{2} + (n_2^0 + s)\sin\phi(s) + n_1^0 \cos\phi(s) - y(s) = H \equiv \text{ constant}. \tag{4.4}$$

Substituting the boundary conditions (4.2) at $s = 0, L$ into (4.4) yields the equations

$$n_1^0 = H, \qquad n_1^0 = -H. \tag{4.5}$$

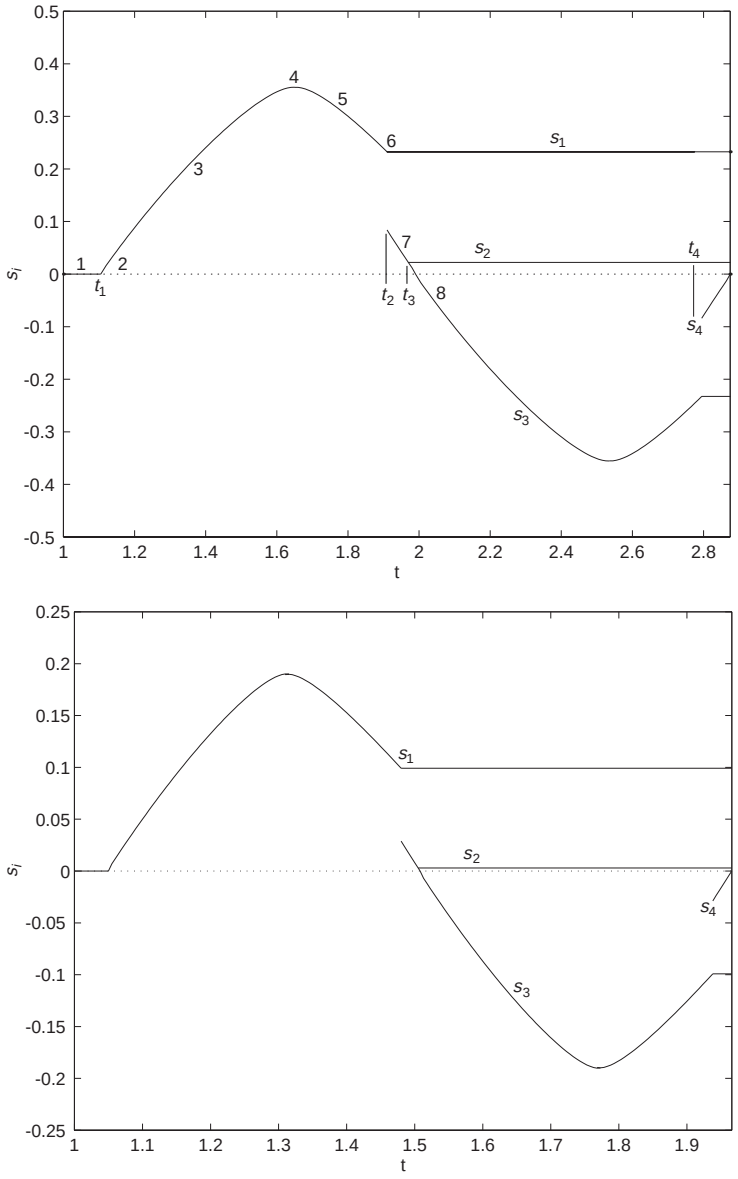

Fig. 5 *The location of the contact lines $s_i(t)$ and the switching points $t_i, i = 1, 2, 3, 4$, as a function of the amount of sheet fed, t, for* (a) $\eta = 10^{-3}$ *and* (b) $\eta = 10^{-4}$. *For $\eta = 10^{-3}$, the positions of the contact lines corresponding to the sequence in Figure* 4 *are also indicated.*

Therefore, $H = 0$, so that $n_1(s) = n_1^0 = 0$ and there are no horizontal forces on the free-standing fold.

To solve the nonlinear boundary value problem (4.1) and (4.2) for the fold shape and the constant L, we use a continuation method similar to that described in section 3.2, implemented in two stages. In the first stage, we consider the feeding of a horizontal sheet lying on the solid plane with the feeding end $s = 0$ clamped and the

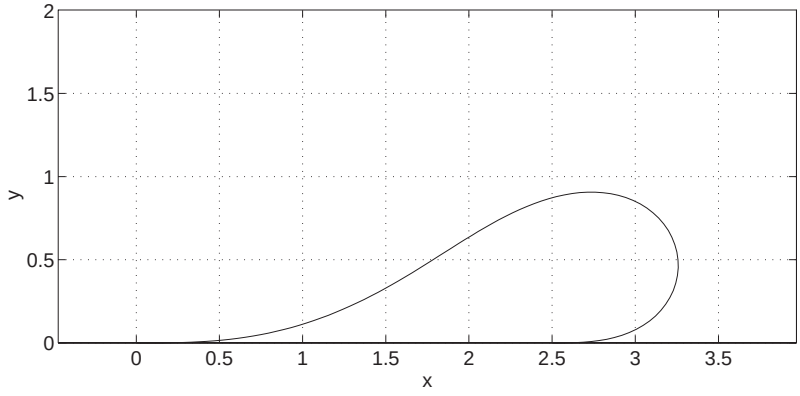

Fig. 6. *The shape of a free-standing fold, computed numerically by solving* (4.1) *and* (4.6).

far end $s = a$ fixed but hinged. Then the boundary conditions (4.2) are replaced by

$$\begin{aligned} &x(0) = 0, \qquad x(a) = 1, \qquad 1 \le a \le L^*, \\ &y(0) = 0, \qquad y(a) = 0, \\ &\phi(0) = \pi, \qquad \phi_s(a) = 0. \end{aligned} \tag{4.6}$$

In the absence of gravity, a perturbation solution to (4.1)–(4.2) for $a = 1+\epsilon, \epsilon << 1$ is given by

$$\begin{aligned} n_1(s;\epsilon) &= \frac{-\pi^2}{4} + O(\epsilon^2), \\ n_2(s;,\epsilon) &= O(\epsilon^2), \\ \phi(s;\epsilon) &= \pi - \epsilon \cos\frac{\pi s}{2} + O(\epsilon^2), \\ x(s;\epsilon) &= s + O(\epsilon^2), \\ y(s;\epsilon) &= \frac{2\epsilon}{\pi} \sin\frac{\pi s}{2} + O(\epsilon^2). \end{aligned} \tag{4.7}$$

Using (4.7) as an initial approximation in COLSYS, we first use a continuation method to find the solution of (4.1) and (4.6) that includes gravity, as in section 3.2. Next, we increase a in steps of 0.1, solving the system at each step until at some value of a that we call L^*, we have $\phi(L^*) = 0$. This completes the first stage. In the second stage, we release the far end of the sheet $s = a$, allowing it to move freely as a is increased beyond L^*. This corresponds to replacing the condition $x(a) = 1$ in (4.6) by $\phi(a) = 0$. Using the solution for $a = L^*$ as the initial guess in COLSYS, we follow the deformation of the sheet until $\phi_s(0) = 0$ for some value of a that we call L. The converged solution then gives the free-standing fold determined by (4.1) and (4.2). In Figure 6 we show the computed shape of the fold, which agrees well with the shape of the folds shown in Figures 1h and 1i.

The constant L is found to be 4.6833 so that the characteristic fold length l_f measured along the arc is given by

$$l_f = 4.6833(EI/\rho g)^{1/3}. \tag{4.8}$$

Similarly the maximum height h_f and the maximum width w_f of the fold are given by

$$h_f = .9066(EI/\rho g)^{1/3}, \qquad w_f = 3.2324(EI/\rho g)^{1/3}. \tag{4.9}$$

5. Experiment. Qualitatively, the numerical solution for the evolution of one half-period of a fold, shown in Figure 3, agrees well with observations of the folding of paper sheets, shown in Figure 1. Now we will compare our theoretical predictions for the free-standing fold with the results of some simple folding experiments.

The experiments were done with various types of paper that were unrolled and left hanging for a few hours to straighten them out. We use the simple gravity loaded cantilever beam experiment to determine the stiffness of the paper sheets. It involves measuring the deflection of the free end and using a calibration diagram to read off the stiffness.

Consider a thin sheet of naturally straight paper of length l that is clamped horizontally at the end $s = 0$ and free at the end $s = l$, as is shown in Figure 7a. The equilibrium shape of the sheet of unit dimensionless length and dimensionless stiffness $\eta = EI/\rho g l^3$ is determined by the solution of the equations (2.8) subject to the boundary conditions

$$\begin{aligned} &x(0) = 0, \quad y(0) = 0, \quad \phi(0) = 0, \\ &\phi_s(1), \quad n_1(1) = 0, \quad n_2(1) = 0. \end{aligned} \tag{5.1}$$

As the length of the sheet is slowly increased or as η is decreased, the sheet droops more and more under its own weight. Using the numerical continuation described before, we compute the sequence of solutions parametrized by the length of the sheet l or the stiffness η. Following [6], we calculate $\tan\theta = y(l)/x(l)$, where θ is the angle made by the horizontal axis with the chord from one end of the sheet to the other, and in Figure 7b we plot η^{-1} versus $\tan\theta$.

In the experimental setup, we calculate $\tan\theta$ by measuring the coordinates of the free end $x(l), y(l)$. Using the calibration diagram in Figure 7b, we can then read off $\eta^{-1} = \rho g l^3/EI$. Finally, by determining the mass per unit area ρ of the sheet, we can evaluate the stiffness EI of the sheet and use (4.8) to predict the fold length l_f.

Next, the sheet is folded over and the length of a free-standing fold $\hat{l}_f$ is measured. Table 2 shows the values of the theoretical and experimental fold lengths l_f and $\hat{l}_f$ for three types of paper and plastic sheets. A comparison of the results shows that the predicted fold lengths are in good agreement with the experiments.

6. Postscript. An earlier paper of Lloyd, Shanahan, and Konopasek [7] was brought to our attention after our work was published. It treated numerically the folding of heavy fabric sheets, based on equations equivalent to ours, and obtained many of the same results. Our study goes beyond it in determining the paths of the various contact points as functions of the sheet length, determining the sheet stiffness from the cantilever experiments, comparing the theory with experiments, etc.

Subsequently, we analyzed the related problem of coiling of a flexible rope fed from above onto a horizontal plane [8]. In that case, we considered the time-dependent motion in three dimensions, which becomes steady in a rotating coordinate system. Recently we have studied the analogous problem of coiling of a filament of viscous fluid falling onto a horizontal plane [9].

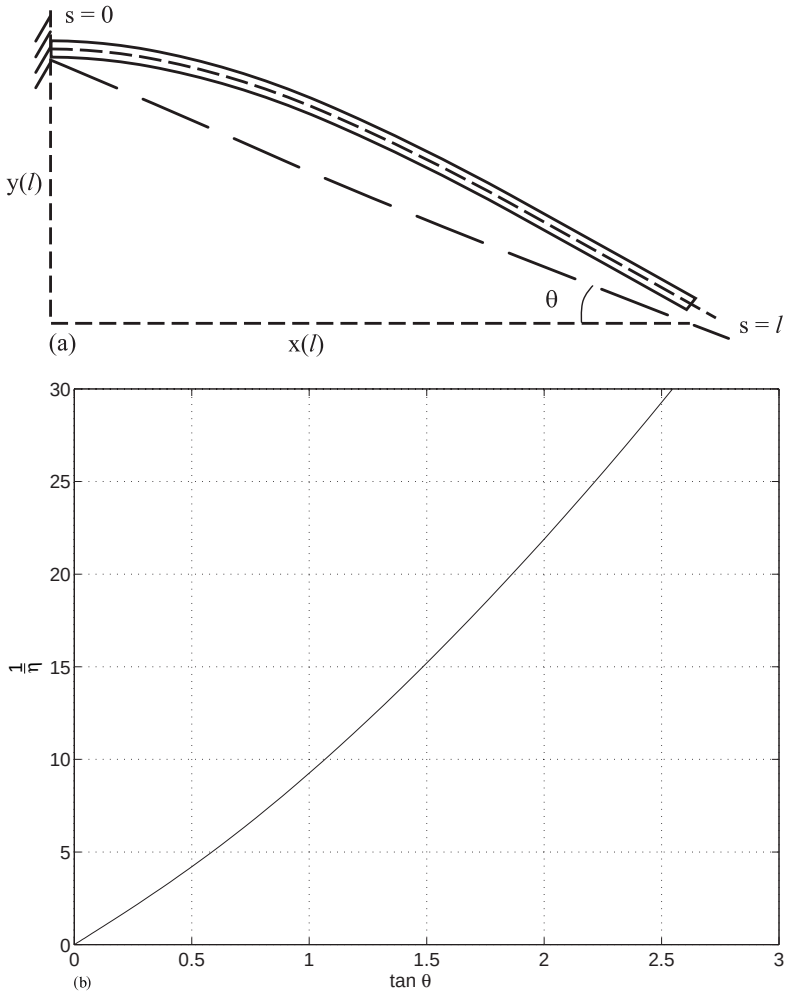

Fig. 7 (a) *Experimental setup and* (b) *calibration diagram for the measurement of the stiffness of a thin sheet.*

Table 2. *Experimental results for free-standing folds.*

$\hat{l}_f(m)$	$l_f(m)$	$\lvert l_f - \hat{l}_f \rvert / l_f$
0.253	0.266	.04
0.622	0.633	.02
0.556	0.540	.03

Acknowledgment. We thank Professor J. R. Ockendon for bringing [1] to our attention.

REFERENCES

[1] A. Friedman, ed., *Mathematics in Industrial Problems, Part* 4, IMA Vol. Math. Appl. 48, Springer-Verlag, New York, 1991, pp. 13–15.

[2] J.O. Cruickshank and B.R. Munson, *Viscous fluid buckling of plane and axisymmetric jets*, J. Fluid Mech., 113 (1981), pp. 221–239.
[3] R.W. Griffiths and J.S. Turner, *Folding of viscous plumes impinging on a density or viscosity interface*, Geophys. J., 95 (1988), pp. 397–419.
[4] A.E.H. Love, *A Treatise on the Mathematical Theory of Elasticity*, 4th ed., Dover, New York, 1927.
[5] U. Ascher, J. Christiansen, and R.D. Russell, *COLSYS, software for boundary value problems*, ACM Trans. Math. Software, 2 (1983), pp. 209–222.
[6] W.G. Bickley, *The heavy elastica*, Phil. Mag., 17 (1934), pp. 603–622.
[7] D.W. Lloyd, W.G. Shanahan, and M. Konopasek, *The folding of heavy fabric sheets*, Int. J. Mech. Sci., 20 (1978), pp. 521–27.
[8] L. Mahadevan and J. B. Keller, *Coiling of flexible ropes*, Proc. Roy. Soc. London A, 452 (1996), pp. 1679–1694.
[9] L. Mahadevan, W.S. Ryu, and A.D.T. Samuel, *Coiling of a viscous filament*, Nature, 391 (1998), p. 140.